Biomaterials Science

ROYAL SOCIETY OF CHEMISTRY

PAPER

View Article Online
View Journal | View Issue

Cite this: *Biomater. Sci.*, 2023, **11**, 7826

X-ray radio-enhancement by $Ti_3C_2T_x$ MXenes in soft tissue sarcoma†

Monika Zimmermann,[a,b] Lukas R. H. Gerken, [a,b] Shianlin Wee, [c] Vera M. Kissling, [b] Anna L. Neuer, [a,b] Elena Tsolaki,[a,b] Alexander Gogos, [a,b] Maria R. Lukatskaya [c] and Inge K. Herrmann *[a,b,d,e]

Radiotherapy is a cornerstone of cancer treatment. However, due to the low tissue specificity of ionizing radiation, damage to the surrounding healthy tissue of the tumor remains a significant challenge. In recent years, radio-enhancers based on inorganic nanomaterials have gained considerable interest. Beyond the widely explored metal and metal oxide nanoparticles, 2D materials, such as MXenes, could present potential benefits because of their inherently large specific surface area. In this study, we highlight the promising radio-enhancement properties of $Ti_3C_2T_x$ MXenes. We demonstrate that atomically thin layers of titanium carbides ($Ti_3C_2T_x$ MXenes) are efficiently internalized and well-tolerated by mammalian cells. Contrary to MXenes suspended in aqueous buffers, which fully oxidize within days, yielding rice-grain shaped rutile nanoparticles, the MXenes internalized by cells oxidize at a slower rate. This is consistent with cell-free experiments that have shown slower oxidation rates in cell media and lysosomal buffers compared to dispersants without antioxidants. Importantly, the MXenes exhibit robust radio-enhancement properties, with dose enhancement factors reaching up to 2.5 in human soft tissue sarcoma cells, while showing no toxicity to healthy human fibroblasts. When compared to oxidized MXenes and commercial titanium dioxide nanoparticles, the intact 2D titanium carbide flakes display superior radio-enhancement properties. In summary, our findings offer evidence for the potent radio-enhancement capabilities of $Ti_3C_2T_x$ MXenes, marking them as a promising candidate for enhancing radiotherapy.

Received 12th April 2023,
Accepted 10th October 2023

DOI: 10.1039/d3bm00607g

rsc.li/biomaterials-science

Introduction

Cancer is the third-leading cause of death in the developed world,[1,2] and while treatments are improving continuously, the side effects often remain severe. Radiation treatment continues to be an integral component of cancer therapy. Approximately half of all cancer patients receive radiotherapy as part of their treatment plan in order to locally destroy or control cancer growth.[3] To improve the therapeutic ratio, *i.e.*, the balance between therapeutic success and side effects, radio-enhancing and/or radio-sensitizing nanoparticles may be introduced into the tumor. Despite encouraging results in both preclinical and more recent clinical studies – including the approval of HfO_2 nanoparticles as radio-enhancers in the treatment of soft tissue sarcoma[4,5] – there is a lack of mechanistic and comparative studies. This scarcity largely precludes rational selection of material candidates.[6,7]

The current understanding suggests that the radio-enhancement mechanism relies on the much higher photoelectric cross-section of high-*Z* nanoparticles, compared to that of soft tissue, at photon energies up to several hundred keV.[8,9] The ejection of an inner-shell electron close to the atomic nucleus leads to a cascading emission of several low-energy electrons (known as the Auger cascade) when the electron vacancy is refilled. These electrons interact with the cell environment surrounding the nanoparticles, causing the radiolysis of water, which is the cells' main constituent. This leads to the formation of reactive oxygen species (ROS).[9,10] ROS, in turn, cause damage to DNA, the cell membrane, and other vital cell components, including mitochondria.[11] In addition to material effects, biological factors such as the cells' suscepti-

[a]*Nanoparticle Systems Engineering Laboratory, Institute of Energy and Process Engineering (IEPE), Department of Mechanical and Process Engineering (D-MAVT), ETH Zurich, Sonneggstrasse 3, 8092 Zurich, Switzerland.*
E-mail: inge.herrmann@empa.ch, ingeh@ethz.ch, inge.herrmann@balgrist.ch, inge.herrmann@uzh.ch; Tel: +41 (0)58 765 7153
[b]*Particles-Biology Interactions, Department of Materials Meet Life, Swiss Federal Laboratories for Materials Science and Technology (Empa), Lerchenfeldstrasse 5, 9014 St Gallen, Switzerland*
[c]*Electrochemical Energy Systems Laboratory, Institute of Energy and Process Engineering (IEPE), Department of Mechanical and Process Engineering (D-MAVT), ETH Zurich, Sonneggstrasse 3, 8092 Zurich, Switzerland*
[d]*The Ingenuity Lab, University Hospital Balgrist, Balgrist Campus, Forchstrasse 340, 8008 Zurich, Switzerland*
[e]*Faculty of Medicine, University of Zurich, Rämistrasse 71, 8006 Zurich, Switzerland*
† Electronic supplementary information (ESI) available. See DOI: https://doi.org/10.1039/d3bm00607g

bility to radicals and their DNA repair capacity may also contribute to the overall treatment response and success.[12–15] At clinically used higher irradiation energies, *i.e.*, in the MeV range, the photoelectric effect becomes negligible.[16] Catalytic effects,[6] as well as biological sensitization,[15] have been identified as driving mechanisms for radio-enhancement, either *via* ROS production (chemical enhancement) or through cellular pathways (biological sensitization). Nanoparticles capable of altering intrinsic cell radiosensitivity by inhibiting specific targets linked to treatment resistance hold great promise. However, a deeper mechanistic understanding is still needed.[7]

Historically, the radio-enhancement field has been strongly focused on gold nanomaterials.[8,17–20] The prevailing hypothesis was that gold atoms, having a high atomic number (Z), would interact strongly with photon radiation compared to cell tissue/water. Indeed, the probability of the photoelectron absorption directly scales with $(Z/E)^n$, where n is a coefficient that varies between 3–4, and E is the incoming photon energy.[21] While the main focus of the field has been on high-Z materials, there is increasing evidence that certain lower-Z materials may offer additional benefits due to radiocatalytic activity,[6] especially at high photon energies. Catalytically active candidate systems include, amongst others, titanium-based materials.[6,22] Due to the surface-specific nature of the catalytic enhancement, the morphologies and architectures enabling maximization of the number of accessible catalytically active sites seem particularly appealing. Thus, nanomaterials with ultra-high specific surface area become a natural choice. Among such materials, MXenes, and in particular $Ti_3C_2T_x$ single flakes, are promising candidates due to their high cytocompatibility.[23,24] MXenes are a relatively new class of 2D transition metal carbides and carbonitrides[25] with a general formula of $M_{n+1}X_nT_x$, where $n + 1$ (n = 1–4) layers of early transition metals (M) are interleaved with n layers of carbon or nitrogen (X). T_x represents the surface terminations, such as O, OH, F, and/or Cl, which are bonded to the outer M layers. In the delaminated form of (hydrophilic) single 2D flakes, $Ti_3C_2T_x$ MXenes satisfy some necessary and important criteria for drug formulation, including water-dispersibility, tailorable size and acceptable stability. $Ti_3C_2T_x$ MXenes have already been successfully employed for photothermal therapy applications,[26] also in combination with chemotherapeutics,[27] or modified with iron oxide for theranostics.[25] Also MXenes of other compositions, including $Ta_4C_3T_x$, have been engineered for similar applications.[28] MXenes have also shown promising antibacterial properties,[29] making them a very versatile material class with a diversity of biomedical applications. However, the utility of MXenes in the realm of radiotherapy remains largely unexplored. Given the established practices of direct intratumoral injection or peritumoral delivery of radio-enhancers, such as HfO_2 nanoparticles, MXenes could present a highly promising avenue for further application in radiotherapy.

In this work, we demonstrate promising radio-enhancement properties for $Ti_3C_2T_x$ MXenes in human soft tissue sarcoma cells and high cytocompatibility in absence of irradiation. We show that $Ti_3C_2T_x$ MXenes fulfill key requirements, including low toxicity in absence of ionizing radiation and in non-cancerous cells, as well as promising radio-enhancement properties in carcinoma cells, supporting the investigation and exploitation of this emerging class of materials for biomedical use.

Results & discussion

Physicochemical characterization of MXenes and dispersant-dependent oxidation

Multilayered and delaminated $Ti_3C_2T_x$ MXenes were synthesized according to previously reported procedures.[30,31] Briefly, Ti_3AlC_2 was etched with hydrochloric acid during 24 h before being thoroughly washed with deionized water and delaminated with lithium chloride. X-ray diffraction (XRD) patterns, Raman and inductively coupled plasma spectroscopy (ICP) analysis of synthesized $Ti_3C_2T_x$ MXenes confirm its phase purity and absence of unreacted Ti_3AlC_2 precursor or oxidized phases such as TiO_2 (Fig. 1a and b). While the as-synthesized $Ti_3C_2T_x$ phase shows a characteristic layered structure, single or few-layer flakes of as-synthesized MXenes become the dominant solid species after dispersion in water and sonication for 5 minutes or more. Transmission electron microscopy (TEM) shows such MXene flakes with lateral dimensions of below 4 μm (Fig. 1c).

A clear understanding of MXene aging behavior as function of the environment is imperative, especially as it provides insights concerning the MXene phase present during cell culture and radio-enhancement experiments (*vide infra*). We utilized STEM EDX and TEM to track evolution of the MXene flakes upon aging in different media: water, lysosomal buffer containing citrate,[32] and cell culture medium. Pristine MXene flakes are characterized by a homogeneous lateral distribution of Ti with a minute number of TiO_2 nanoparticles (Fig. 1d of STEM with EDX on fresh MXenes shows some small regions of higher oxygen concentration), however after 1 week of aging at 37 °C of the $Ti_3C_2T_x$ in water dispersions, TiO_2 nanoparticles become a dominant phase and the initially black dispersions gradually turn white, yielding rice-grain shaped rutile-dominant (*ca.* 70% rutile, 30% anatase) nanoparticles (TEM in Fig. 1e and XRD in Fig. 1a). Rapid oxidation of MXenes in water is well-known.[33–37] In contrast, we observe a notably decreased oxidation rate of the MXenes in the media containing antioxidants, *i.e.* artificial lysosomal buffer containing citrate (Fig. 1f) and cell culture media (Fig. 1g), which is in line with other recent reports on antioxidant-containing dispersants.[38] Within a week, MXenes were only partially oxidized and the characteristic morphology of the MXenes was preserved.

For the cytotoxicity and radio-enhancement investigations (described below), fresh and aged MXenes (*i.e.* oxidized for 1 week in water at 37 °C) were compared and benchmarked against titanium dioxide nanoparticles (P90, Evonik, 80% anatase, 20% rutile[39]) that have well-known radio-enhancement properties.[6,40] P90 was selected because of its cytocom-

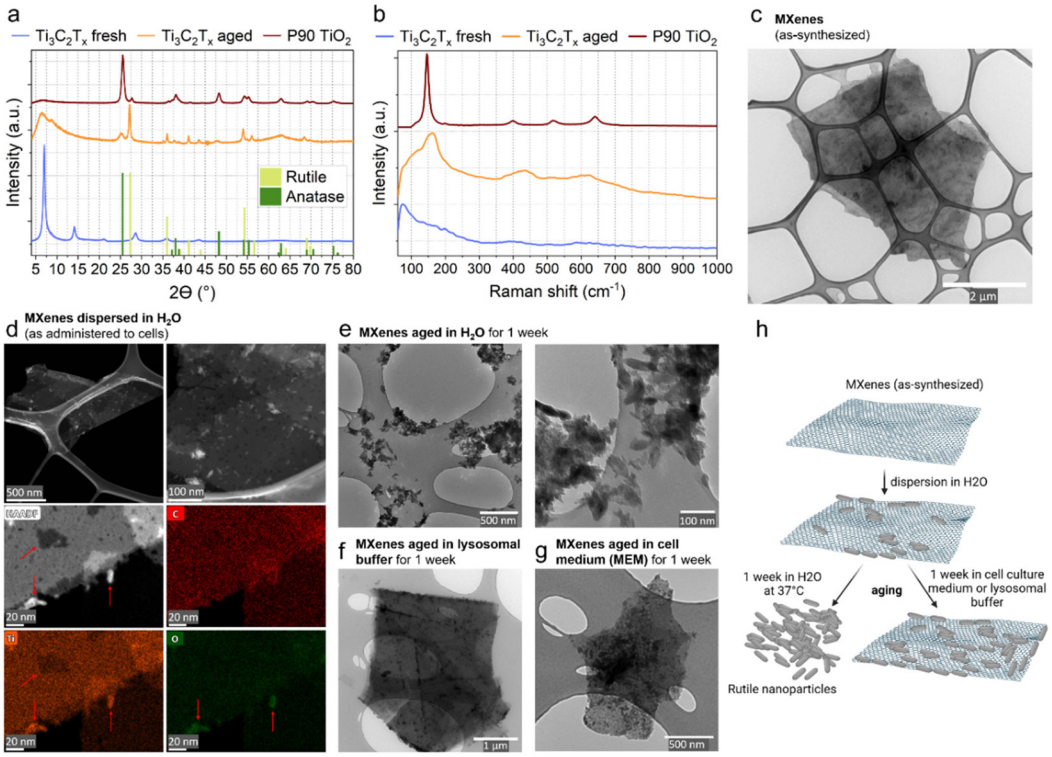

Fig. 1 (a) X-ray diffraction (XRD) patterns of fresh $Ti_3C_2T_x$ MXenes with no evidence for non-Ti contaminants. XRD patterns for aged MXenes shown along with commercially available TiO_2 nanoparticles (P90); a.u.: arbitrary units. (b) Raman spectra for fresh and aged $Ti_3C_2T_x$ MXenes as well as P90 TiO_2 nanoparticles. (c) Transmission electron micrograph of as-synthesized (=fresh) MXenes. (d) Dark-field scanning transmission electron micrographs and corresponding energy-dispersive X-ray spectroscopy maps for carbon (C), titanium (Ti) and oxygen (O) illustrating the partial oxidation of MXenes in water (<1 day). Transmission electron micrographs of MXenes aged in physiologically relevant fluids, including (e) water, (f) lysosomal buffer and (g) cell culture medium over a period of 1 week. (h) Schematic overview illustrating the gradual aging of MXenes in aqueous fluids over time, which can be delayed by addition of antioxidants, such as the ones present in cell culture media or citrate-based lysosomal buffers. In water, MXenes fully oxidize to form rice-grain shaped rutile-dominant nanoparticles over a period of 1 week at 37 °C (denoted as "aged" MXenes, as opposed to "fresh" MXenes).

patibility, favorable cellular uptake and larger specific surface area compared to P25 (BET surface areas of 90–100 $m^2\ g^{-1}$ *vs.* 50 $m^2\ g^{-1}$).

Cytocompatibility, uptake and cellular fate of MXenes

High cell compatibility and uptake are prerequisites for efficient radio-enhancement. Cytotoxicity and cellular uptake were thus quantitatively assessed for fresh $Ti_3C_2T_x$ MXenes, aged (in H_2O) $Ti_3C_2T_x$ MXenes and P90 TiO_2 nanoparticles. Toxicity was measured in human soft tissue sarcoma cells (HT1080, Fig. 2a and b) and normal human fibroblasts (NHDF, Fig. 2c and ESI Fig. S1†) exposed to MXenes for 24 hours in an acute response and a long-term (6 days, full duration of the radio-enhancement study) scenario. While HT1080 cells were included as target cells, normal human fibroblasts served as non-cancerous healthy control cells to account for cancer and healthy cell compatibility. Cell viability was measured based on metabolic activity (adenosine triphosphate (ATP) assay). A dose-dependent viability decrease was observed for the fresh MXenes, however, the overall metabolic activity of the human sarcoma cells remained almost unaffected for concentrations up to 40 µg ml^{-1} and was still >60% of that of untreated control cells for all investigated MXene doses, *i.e.* up to 160 µg ml^{-1} (see Fig. 2a) and exposures for 24 hours. Interestingly, equi-dosed aged MXenes were tolerated by cells even better, showing no effect on cell viability up to 40 µg ml^{-1} at the 24 h time point. The higher effects of fresh MXenes on cell viability can likely be attributed to the following factors: (i) a change in oxygen availability in the cell environment[23,41] through (slow) oxidation of as-synthesized MXenes (in contrast to the more stable aged MXenes); (ii) the sharp edges of MXenes inducing membrane damage;[29,42] or (iii) further more complex (biological) mechanisms. However, oxidative stress caused by MXene exposure has been subject to controversy[29,41,42] and is likely dependent on the cellular environment and exposure times. The P90 TiO_2 nanoparticles were tolerated similarly well as equi-dosed aged MXenes and showed no detectable effect on cell metabolic activity up to concentrations of 320 µg ml^{-1}.

In normal human fibroblasts, both fresh and aged MXenes caused no measurable effect on cell viability and were excellently tolerated up to doses of 160 µg ml^{-1} (see ESI Fig. S1†). This is well in line with previous results indicating increased tolerance of non-cancerous cells towards oxidative stress[43,44]

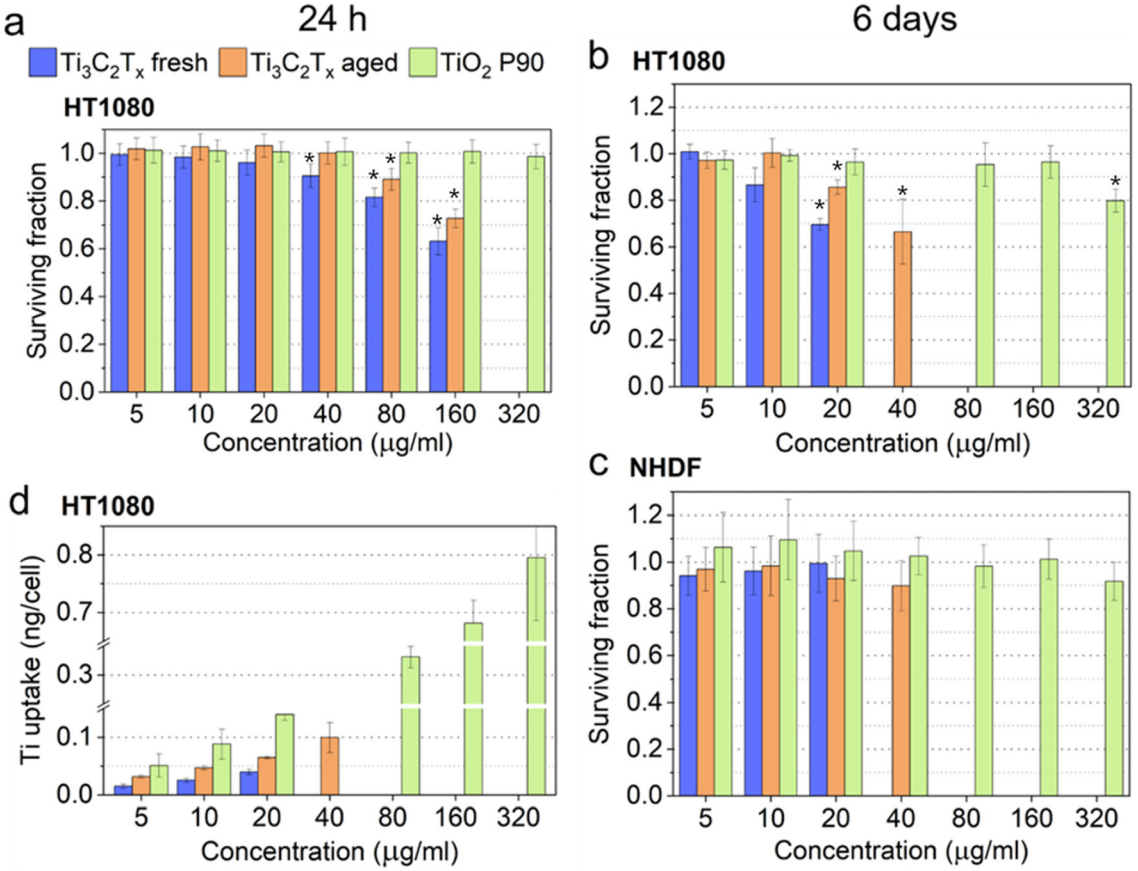

Fig. 2 (a) Cell viability for 24 h and (b) 6 days exposure of human soft tissue sarcoma cells and (c) 6 days exposure of healthy human fibroblasts to fresh $Ti_3C_2T_x$ MXenes, aged $Ti_3C_2T_x$ MXenes and commercial TiO_2 nanoparticles (P90). (d) Uptake of the respective nanomaterials into human soft tissue sarcoma cells after 24 h of incubation, expressed as Ti metal mass measured by inductively coupled plasma spectroscopy. For the uptake experiments as well as the 6 day radio-enhancement and toxicity study, only subtoxic doses (up to 20 μg ml^{-1}) have been included. * in the cell viability plots (a–c) indicates $p < 0.05$ (Bonferroni *post-hoc* corrected) and a significant difference to untreated control cells.

and $Ti_3C_2T_x$ MXenes.[45] With regard to the long-term viability (see Fig. 2b and c), reduction in viability was more pronounced compared to the 24 hours timepoint for both the fresh MXenes, with 6-day viabilities of ~70% for doses of 20 μg ml^{-1} (compared to >95% at 24 h) and aged MXenes with >65% viability for doses of 40 μg ml^{-1} (compared to unaffected cell viability at the 24 h time point). All in all, we observed moderately decreased cell viability at 24 hours and more pronounced long-term effects of MXene-related materials in sarcoma cells and an overall attenuated response in healthy fibroblasts. These findings further support the postulated selective toxicity of $Ti_3C_2T_x$ towards cancerous cells.[45]

To account for potentially different sedimentation and uptake rates for the different materials,[40] the cell viability results were also contextualized with cellular uptake data. Elemental analysis based on inductively coupled plasma mass spectroscopy (ICP-OES) shows a cell-associated Ti-content (metal mass) of 0.015–0.04 ng per cell for the fresh $Ti_3C_2T_x$ MXenes, about double of it for aged MXenes, and even higher Ti-content for P90 TiO_2 nanoparticles with 0.06–0.8 ng per cell for concentrations from 5–320 μg ml^{-1}, with a non-linear increase (Fig. 2d). The uptake results for TiO_2 nanoparticles are well in line with previous work,[40] attesting to the high reproducibility of these cellular uptake measurements.

The interaction with cells and the cellular uptake of the $Ti_3C_2T_x$ MXenes was further investigated by TEM and STEM with EDX to investigate the intracellular accumulation and account for any potential biotransformation (*e.g.* oxidation, changes in elemental composition, or morphological changes, Fig. 3 and ESI Fig. S2†). MXenes can be readily localized intracellularly, and their characteristic sheet-like structure is preserved for MXenes taken up by cells. While most intracellular MXenes display lateral dimensions of below 4 μm (also caused by the sectioning during TEM/STEM sample preparation), occasionally, large arrays of sheets exceeding dimensions of 10 μm are observed intracellularly. These findings align closely with observations of other 2D materials, such as graphene sheets,[46,47] which are internalized through both endocytosis and phagocytosis processes.[48] In contrast, the aged MXenes have lost their characteristic sheet-like form and mostly consist of loosely clustered rice-grain shaped TiO_2 particles, or in rare cases remainders of sheets covered with TiO_2.

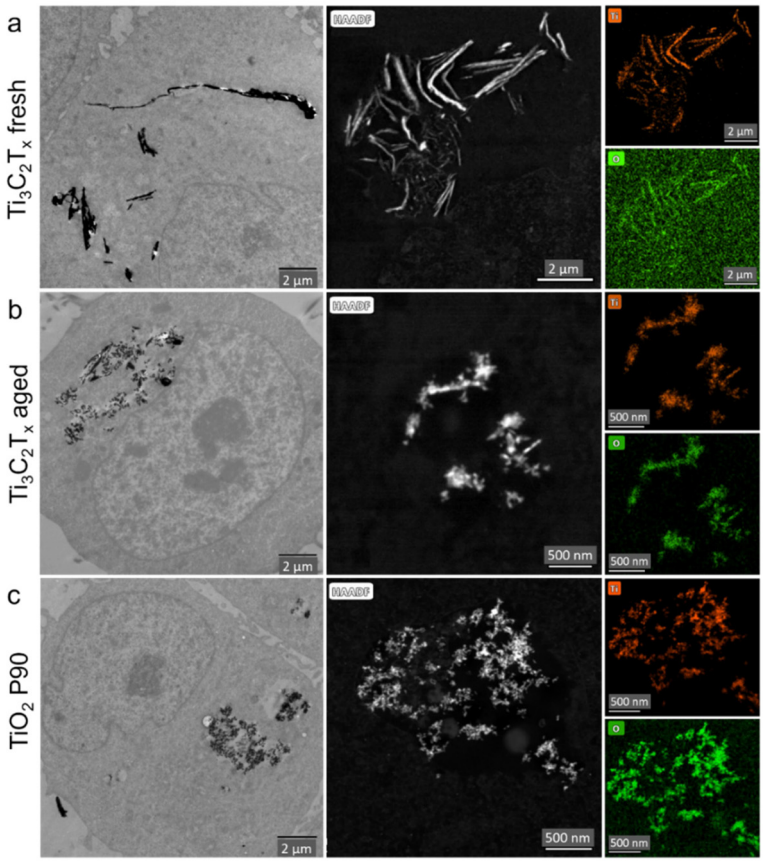

Fig. 3 Left: Transmission electron micrographs of human sarcoma cells after 24 hours of incubation with (a) fresh $Ti_3C_2T_x$ MXenes, (b) aged $Ti_3C_2T_x$ MXenes (aged for 1 week at 37 °C in milliQ H_2O), and (c) P90 TiO_2 nanoparticles. Center: High-angle annular dark field (HAADF) scanning transmission electron micrographs. Right: Corresponding energy-dispersive X-ray spectroscopy (EDX) maps of Ti and O. Fresh MXenes show an overall lower oxygen content compared to aged MXenes or TiO_2 nanoparticles. Aged MXenes present a morphology similar to P90 TiO_2 nanoparticles.

TEM and STEM micrographs show fresh and aged MXenes localized in the cytoplasm, mostly as agglomerates. The intracellular MXenes, whether fresh or aged, retain a morphology closely resembling the original materials – sheets for the former and particles for the latter. When introduced to cell cultures, there was no evident major oxidation in the fresh MXenes, as confirmed by morphological and semi-quantitative compositional analysis using EDX, with the oxygen content being comparable to the background. The aged MXenes present a morphology, elemental contents and a cellular distribution more similar to the P90 TiO_2 nanoparticles rather than the original MXenes, which showed an overall lower oxygen content.

The STEM data also hint a possible reason for the lower uptake of fresh $Ti_3C_2T_x$ MXenes caused by their larger (longitudinal) size (~1–3 µm) compared to their (partially) oxidized counterparts and the fully oxidized P90 TiO_2.[49] P90 TiO_2 nanoparticles were taken up by cells most likely *via* an endocytic pathway,[50,51] and formed intracytoplasmic agglomerates contained in membrane-bound vesicles with characteristic sizes of ~500–2000 nm, which is well in line with previous studies on flame-sprayed titania nanoparticles.[40] The aged MXenes show intracellular agglomeration and distribution similar to the TiO_2 nanoparticles. Importantly, these electron microscopy investigations show that nanomaterials were exclusively localized in the cytoplasm and no evidence for particles in the nucleus was found in any of the investigated samples. This is well in line with the reported size threshold of the nuclear pores of 9 nm.[52]

In vitro dose enhancement effects

Following the investigation of the $Ti_3C_2T_x$ MXene cytotoxicity and cellular uptake, the radio-enhancement performance in human sarcoma (HT1080) and fibroblast (NHDF) was quantified for both fresh and aged $Ti_3C_2T_x$ MXenes, and benchmarked against commercial TiO_2 nanoparticles (Fig. 4 and ESI Fig. S3†). After 24 h-incubation with the respective nanoparticles at concentrations ranging from 5–320 µg ml^{-1}, HT1080 cells were irradiated with 0, 2, 4, 6 and 8 Gy with a 150 kVp X-ray beam and analyzed 5 days later. The surviving fraction relative to the non-irradiated control cells exposed to the same concentration of the corresponding nanoparticles decreased in a logarithmic fashion, which can be fitted with the linear quadratic model commonly used in radiobiology.[53] Amongst the three different materials investigated, the fresh $Ti_3C_2T_x$ MXenes showed the most pronounced dose-dependent

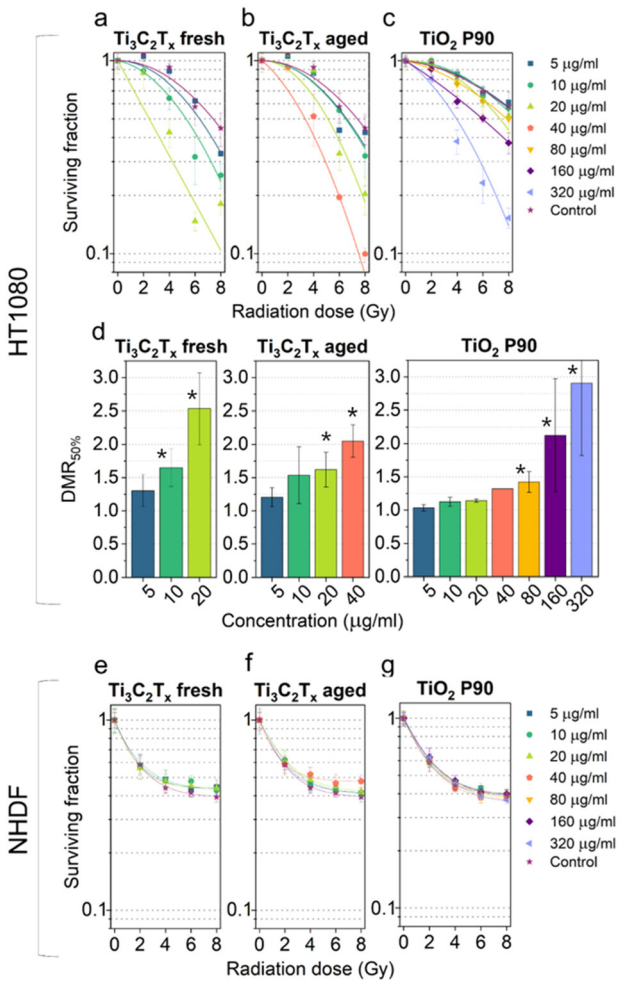

Fig. 4 Surviving fractions of human soft tissue sarcoma cells irradiated at different X-ray doses, relative to untreated, non-irradiated control, treated with (a) fresh $Ti_3C_2T_x$ MXenes, (b) aged $Ti_3C_2T_x$ MXenes and (c) TiO_2 (P90). (d) Dose-modifying ratio (DMR) at 50% cell survival for aforementioned particle types and different concentrations in HT1080 (* indicates $p < 0.05$). (e–g) Surviving fractions of normal human dermal fibroblasts irradiated at different X-ray doses, relative to untreated, non-irradiated control, treated with (e) fresh $Ti_3C_2T_x$ MXenes, (f) aged $Ti_3C_2T_x$ MXenes and (g) TiO_2 (P90).

radio-enhancement effects in radio-resistant human soft tissue sarcoma cells, followed by the aged MXenes (Fig. 4a–c). At the highest tolerable nanoparticle concentration (defined as >80% viability of cells after 24 h exposure) and an irradiation dose of 8 Gy, <20% of the cells – compared to the nanoparticle-treated control cells – survived. The dose-modifying ratio (DMR) for 50% cell death reached 2.5, thereby surpassing previously reported values for TiO_2 studied in similar conditions.[6]

An interesting observation can be made based on the correlation between the effectively taken up nanoparticle concentration and the ensuing radio-enhancement effect: by assessing the cellular uptake of Ti metal atoms from MXenes and P90 (as shown in Fig. 2d) and considering the respective molar masses of both particle types, one can deduce that at an initial concentration of, for instance, 20 µg ml^{-1}, cells take up roughly 10 times more P90 than aged MXenes, and about 20 times more than fresh MXenes. However, despite this, the radio-enhancing potential of both fresh and aged MXenes at the 20 µg ml^{-1} concentration was significantly greater than that of P90 TiO_2, suggesting a higher activity for the MXenes (see also ESI Fig. S4†). The $DMR_{50\%}$ values obtained for fresh and aged MXenes also exceed the ones previously observed for TiO_2 and HfO_2 nanoparticles in an equivalent setting.[6] Taken together, the respective surviving fractions at different nanoparticle concentrations and the effective uptake quantities indicate a significantly higher radio-enhancement efficiency per nanoparticle mass of MXenes than of P90 and other previously investigated metal oxides (HfO_2, WO_3) and metals (Au). While metal oxides and gold affect the cell viability to a lesser extent than the fresh MXenes, and thus can potentially be applied at higher doses, the $DMR_{50\%}$ values of the latter does not exceed the one observed for low-dose MXenes ($DMR_{50\%}$ of 2.5) even at maximally tolerated doses.[6] Importantly, equivalent dose administration of fresh and aged MXenes to normal human dermal fibroblasts does not lead to any measurable radio-enhancement (Fig. 4e–g, $DMR_{50\%} \approx 1$ for all nanomaterials and concentrations), suggesting a very promising therapeutic ratio.

The strong radio-enhancement effects of MXenes may be caused by their ability to generate radicals when irradiated,[23,54] as well as their ability to interfere with the natural antioxidant machinery of the cells. As the MXenes only contain low-atomic number elements (Ti, C, and potentially O), no significant physical dose enhancement is expected. This can further be supported by mass calculations of the macroscopic DEF for a Ti–water mixture to be expected from a 150 kVp source based on physical enhancement as well as Monte Carlo (MC) simulations. Due to the macroscopic material homogenization the macroscopic DEF calculations overestimate the DEFs compared to MC simulations based on actual cell geometries by Gerken *et al.*,[6] which showed no relevant physical enhancement of Ti-related nanoparticles (TiO_2 and TiN) for the 150 kVp source (ESI Fig. S5†). The high dose enhancement observed in cell experiments for low mass fractions of MXenes compared to the expectedly low physical enhancement, along with the considerably lower (DEF ≈ 1) radio-enhancement effects observed in healthy fibroblasts, which are much more resistant towards oxidative stress,[55] strongly support a radical-based mechanism. Indeed, in our experiments where the antioxidant dimethyl sulfoxide (DMSO) was added to the cell cultures, the radio-enhancement was partially attenuated for both MXenes and P90, supporting an OH^--mediated radio-enhancement mechanism for fresh MXenes (ESI Fig. S6†). Mechanistically, these pronounced radio-enhancement effects are further supported also by recent findings suggesting that MXenes may hinder the activity of antioxidant enzymes and make ROS accumulate intracellularly causing oxidative damage to biomacromolecules and cell membranes.[56] It has further been shown that MXenes treatments may damage the antioxidative system and reduce superoxide dismutase (SOD)

activity leading to the elevated intracellular ROS level and oxidative damage.[56] In sum, this research underscores the promising radio-enhancement potential of MXenes, particularly noting a more pronounced enhancement effect in cancerous cells compared to healthy ones. Future endeavors could delve into addressing the delivery challenges and deepening our understanding of the underlying mechanisms based on emerging ROS detection technologies.

Conclusions

Taken together, the present work shows potent radio-enhancement properties for $Ti_3C_2T_x$ MXenes, and to a lesser extent also for aged (oxidized) $Ti_3C_2T_x$ MXenes at subtoxic concentrations. Interestingly, the MXenes do not undergo complete oxidation in the cell cultures and their characteristic sheet structure remains well preserved, in contrast to MXenes exposed to antioxidant-devoid aqueous environments. The high dose enhancement ratios enabled by MXenes together with their negligible toxicity towards non-cancerous cells at therapeutically effective concentrations make them a promising candidate material for radiotherapy augmentation. The fact that a substantially larger mass (approx. 8 times more) of P90 TiO_2 is needed to achieve the same radio-enhancement effect as with oxidized $Ti_3C_2T_x$ suggests that the effect from the latter does not (only) stem from the TiO_2 formed on top of the MXene sheets during partial oxidation. This indicates that other mechanisms of radio enhancement might be at play, such as reactive oxygen species generation and interference with the antioxidant machinery of the cells. While a deeper mechanistic understanding of the ROS production would be of great interest, commonly used fluorescence ROS assays show strong assay interference, therefore alternative strategies are warranted. In addition, the identification of optimal routes for MXenes delivery is a major research priority, extending on strategies such as intratumoral injection (similarly to what is done for hafnium dioxide nanoparticle delivery to soft tissue sarcoma tumors today[57]) or peritumoral delivery *via* catheters, as well as encapsulation for the targeting of difficult-to-reach tumors. Importantly, comparative studies,[58] such as this one including TiO_2 benchmarks, and an in-depth understanding of toxicity and long-term effects are imperative for the rapid, evidence-based and sustainable advancement of the nanomaterial radio-enhancement field.

Materials & methods

Materials

Titanium dioxide nanoparticles (Aeroxide®, P90) were obtained from Evonik Industries AG (Essen, Germany).

$Ti_3C_2T_x$ MXenes synthesis

$Ti_3C_2T_x$ MXene colloidal suspension was produced similarly to previous reports.[30,31] Briefly, 1 g of Ti_3AlC_2 powder (Carbon-Ukraine, <44 μm particle size) was added gradually to a mixture of 6 ml DI water, 12 ml of concentrated hydrochloric acid (HCl, Sigma-Aldrich, 35%) and 2 ml of concentrated hydrofluoric acid (HF, Sigma-Aldrich, 48 wt%). Then, the mixture was stirred at 300 rpm under a constant temperature of 25 °C for 24 hours. After etching, the multilayer $Ti_3C_2T_x$ powder was washed with DI water several times *via* centrifugation at 3500 rpm for 5 min until neutral pH was reached. The obtained multilayer $Ti_3C_2T_x$ powder was delaminated by using 1 g of lithium chloride (LiCl, Carl Roth, 99%) in 50 ml of DI water. After the addition of $Ti_3C_2T_x$, the mixture was then stirred at 300 rpm, for 24 hours at 25 °C. Then, the solution was centrifuged at 3500 rpm for 10 min for several times until the supernatant became dark. The dark solution containing the delaminated single/few layer flakes was collected. To obtain aged MXenes, fresh MXene dispersion was diluted 1 : 1 with milliQ water and put at 37 °C for 7 days while being constantly slightly shaken.

Nanomaterial characterization

Transmission electron microscopy (TEM) imaging was performed on a Zeiss EM 900 microscope (Carl Zeiss Microscopy GmbH, Germany) at 80 kV. Samples of as-synthesized MXenes were prepared by drop-casting a dispersion of 50 μg ml^{-1} in ultrapure (milliQ) H_2O after 5 min sonication quickly onto a lacey carbon-coated grid (200 mesh copper, EM Resolutions). The grid was then immediately placed into a vacuum chamber to prevent further oxidation in air. For a MXenes sample as administered to cells, the MXenes were dispersed in milliQ H_2O for 2 h by sonication and then drop-casted onto a lacey carbon-coated grid (200 mesh copper, EM Resolutions) at 0.1 μg ml^{-1}. For aged MXenes samples, a stock of 0.5 mg ml^{-1} was incubated for 1 week at 37 °C in milliQ H_2O, artificial lysosomal buffer (citric acid buffer 0.01 M, pH 4.5) or cell culture medium (Eagle MEM, Sigma-Aldrich or Gibco), diluted in milliQ H_2O to 50 μg ml^{-1}, drop-casted onto a holey carbon-coated grid (200 mesh copper, EM Resolutions) and washed three times with milliQ H_2O. These grids were then also stored in a vacuum chamber. Dark-field scanning transmission electron microscopy and corresponding energy-dispersive X-ray spectroscopy (EDX) mapping of the described grids with MXenes in water (<1 day) as administered to cells and MXenes aged for 1 week in biological fluids, including milliQ H_2O, lysosomal buffer and cell culture medium was performed on a FEI Talos F200X (Thermo Fisher Scientifc) microscope at 200 kV. X-ray diffraction patterns were obtained with a Bruker 2D Phaser with a step size of 0.01°. For the Raman measurements of fresh and aged MXenes a WiTec Raman alpha 300R microscope was used with a 63×/1.0 M27W "Plan-Apochromat" water immersion lens (Zeiss, #421480-9900-000) and a 532 nm laser at a laser power 20 mW and an integration time of 2 s and 10 accumulations. Cosmic ray removal and smoothing were carried out using the Project 5 WiTec software. In addition, TiO_2 P90 was analysed on a Renishaw "inVia" with the "Wire" software (Renishaw plc, Gloustershire, Great-Britain).

Cell lines and culture conditions

Human soft tissue sarcoma HT1080 cells (ATCC®CCL121TM) were cultured in minimum essential medium Eagle (MEM, Sigma-Aldrich or Gibco) supplemented with 10% fetal bovine serum (FBS, Sigma-Aldrich), 1% L-glutamine (Sigma-Aldrich), 1% non-essential amino acids (NEAA, Sigma-Aldrich), 1% penicillin–streptomycin (PS, Sigma-Aldrich) and 1 mM sodium-pyruvate at 37 °C under a humidified atmosphere containing 5% CO_2. Subculturing was conducted at 70–80% confluency by treatment with 0.5% Trypsin-EDTA (Sigma-Aldrich). Normal human dermal fibroblast cells (NHDF, PromoCell, Germany) were cultured in Dulbecco's Modified Eagle's medium – high glucose (#RNBG3787, Sigma-Aldrich) supplemented with 10% fetal calf serum (FCS), 1% PS and 1% L-glutamine. Cells were sub-cultured once a week upon 80% confluence.

Cell sample preparation for S/TEM imaging

To image intracellular nanoparticles, 150′000 cells were seeded in T25 flasks, diluted in 8 ml cell medium. After letting them attach overnight, the relevant nanoparticle suspension (diluted in ultrapure water) was added such as to reach a final nanoparticle concentration of 20 μg ml^{-1} in the flask. We let them incubate for 24 h, then washed the cells twice with PBS, followed by detaching them with trypsin (Accutase, Sigma-Aldrich) and washing them again with PBS. After centrifugation, 2.5% Glutaraldehyde (Sigma-Aldrich) in 0.1 M Na-cacodylate buffer (Electron Microscopy Sciences) was added to fix the cell pellets for one hour, followed by washing away the fixation solution with 0.1 M Na-cacodylate buffer. To store the cell pellets for later embedding procedures, 0.1 M Na-cacodylate was added, and the samples were centrifuged and subsequently stored at 4 °C for several days. The cell pellets were then stained with 1% osmium tetroxide (Electron Microscopy Sciences) in 0.1 M Na-cacodylate buffer for one hour in the dark at room temperature; this step was omitted for fresh and aged MXenes as osmium was observed to accumulate especially along fresh MXenes (see SI). After washing with water, the cell pellets were gradually dehydrated *via* an Ethanol series (30%, 50%, 70%, 90%, 100%), then incubated in 1 : 1 ethanol 100% and Epon 812 substitute resin (Epoxy embedding kit 45359, Sigma-Aldrich) for one hour and subsequently left in 100% Epon overnight. The cell pellets were then embedded into molds with fresh Epon and cured in the oven at 60 °C for at least 2 days. Thin sections of 70–100 nm thickness were then cut with an ultra 35° diamond knife (DiATOME) from the resin blocks with an ultramicrotome (Leica EM UC6) and placed onto Formvar-coated copper grids (200 mesh copper, EM Resolutions). The sections of fresh MXenes and P90 were stained with 2% uranyl acetate for 15 min and 1 min with lead citrate to enhance cell contrast. All sections were then imaged by TEM using a Zeiss EM 900 microscope (Carl Zeiss Microscopy GmbH, Germany) at 80 kV and by high-angle annular dark-field (HAADF) scanning transmission electron microscopy (STEM) with energy-dispersive X-ray spectroscopy (EDX) using a FEI Talos F200X (Thermo Fisher Scientific) microscope at 200 kV. For fresh MXenes embedded in cells, standard embedding protocols including osmium staining was performed at first, however, due to Osmium accumulation around MXenes (see ESI Fig. S2†), osmium-free embedding was used in order to avoid confounding of the images by Os.

Cell viability assessment and number of cell quantification

The CellTiter-Glo (CTG) assay (CellTiter-Glo® Luminescent Cell Viability Assay, Promega, G7571) was employed to measure the viability of cells, following the manufacturer's specifications with slight adaptions to our setup. CTG buffer and substrate were thawed and mixed. For viability measurements after irradiation where 48-well plates were used, of the 500 μl total cell medium per well, 300 μl were replaced by 200 μl CTG reagent. For 24 h cytotoxicity measurements, where 96-well plates were used, after washing of the nanoparticles 100 μl of MEM and 100 μl of CTG were added to each well. After incubation in the dark on a shaker for 20 min and equilibration for 30 min in the dark, luminescence (integration time 1 s) was measured with a microplate reader (Mithras LB 943 Multimode). An in-house made black titanium adapter was applied to eliminate crosstalk between the transparent wells. This method was established in an earlier study[6] using a very similar setup, where an even distribution of the luminescence signal on the plate was achieved through elimination of the luminescence cross-talk by the adapter.

Irradiation conditions

For all X-ray irradiation experiments, an in-house made MPPA phantom consisting of two equally sized slabs (4 × 40 × 40 cm^3, for details see Gerken *et al.*[6] (Fig. S15†)) was placed above and beneath the 48-well plates containing the cells (TPP, Techno Plastic Products AG, Switzerland). The photons thereby went through ∼4 cm PMMA material before reaching the cover of the well plate. A tube source (Seifert ISOVOLT 450, GE Sensing & Inspection Technologies GmbH, Germany) with a 7 mm beryllium filter window was placed 50 cm above the lower phantom slab and operated at 150 kV and 20 mA. The dose rate deposited on the well plate was ∼1.5 Gy min^{-1}, which was measured with a calibrated ionization chamber (N31003, PTW, Freiburg, Germany) that was guided *via* an 8 mm inlet to the center of the plate and was connected to a UNIDOS dosimeter (PTW, Freiburg, Germany). This allowed to measure the dose rate deposited in the middle of the phantom alone, and during the cell irradiation to monitor the dose supply.

Cell irradiation and *in vitro* dose-enhancement quantification

48-well plates were used to seed 2000 HT1080 or NHDF cells diluted in 300 μl cell medium per well, and let to adhere for 24 h. Then, 200 μl of nanoparticle dispersion (or control solution) was added to each well such as to reach the desired final nanoparticle concentrations. The different nanoparticle solution were prepared by mixing the nanoparticle stock solution

(nanoparticles dispersed in milliQ water and sonicated) with cell medium and milliQ water such as to have a constant water content of 10% in each solution. The control (*i.e.* nanoparticle-free) solutions were made of cell medium and 10% milliQ water. After letting the cells incubate with the nanoparticles for 24 h, they were washed twice with 250 μl PBS, and 500 μl cell medium was added to each well. The travel time from the incubator to the irradiation facility was ~1 h, during which the cells were kept in a cooled box, and equilibrated to room temperature again before irradiating them. They were transported again in a cooled box back to the incubator. Every 2 days, cell medium was replaced, and on the 5th day (for HT1080) or 7th day (for NHDF) after irradiation, cell viability was measured with the CellTiter-Glo® assay. One biological repeat per nanoparticle concentration consisted of triplicates (n = 3), and for control cells of sextuplicates (n = 6). A linear relation between luminescence and number of cells was assumed, based on previous observations. The surviving fraction of cells, SF, was computed for a given radiation dose D (measured in Gy), as

$$\mathrm{SF}(D) = \frac{\#\ \text{luminescence}(D, \text{with or without NPs})}{\#\ \text{luminescence}(D = 0\ \text{Gy}, \text{with or without NPs})}$$

The SF for 0, 2, 4, 6 and 8 Gy was fitted with the linear quadratic model using Origin (OriginLab Corp, MA, USA):

$$\mathrm{SF} = \mathrm{e}^{-\alpha D - \beta D^2}$$

where α and β are two constant parameters for a given biological situation.

The dose-modifying ratio (DMR) at lethal doses leading to 50% cell survival ($LD_{50\%}$) is defined as

$$\mathrm{DMR}_{50\%} = \frac{\mathrm{LD}_{50\%}(\text{without NPs})}{\mathrm{LD}_{50\%}(\text{with NPs})}$$

Cell digestion and nanoparticle uptake quantification using ICP-OES

To analyze the quantity of nanoparticles effectively taken up by the cells, cells were seeded, let to attach for 24 h, and again incubated with nanoparticles for another 24 h, as in the radio-enhancement experiments described above. Consequently, they were washed twice with 250 μl PBS, and trypsinized (80 μl). To stop the trypsination, 220 μl of cell medium was added and the cells were transferred to Eppendorf tubes and stored at −20 °C. Since the number of cells per well was needed to compute the uptake per cell, three experimental wells with control cells were pooled, centrifuged at 200g for 5 min and counted using a hematocytometer, repeating the operation twice. The stored cells (300 μl, corresponding to ~6500 cells) were digested in 1 ml HNO_3, 3 ml HCl and 0.5 ml HF during a 1 h bath sonication treatment at room temperature. Samples containing $Ti_3C_2T_x$ MXenes were additionally treated in a pressurized microwave (Ultraclave, MLS GmbH) at 250 °C and 120 bar pressure for 18 minutes. Afterwards, all samples were filled up to 50 ml with milliQ water and their $Ti_3C_2T_x$ MXene and P90 TiO_2 content determined using an Agilent 5110 ICP-OES (Agilent Technologies, Santa Clara, USA). To build ICP-OES elemental standard curves, ionic metal standards of Ti and Al were prepared matrix-matched to the samples in concentrations from 0.01 to 10 ppm. A 1 ppm quality control (IV71B, Inorganic Ventures, Christiansburg, VI, USA) served as reference and ensured correctness of the standard curve. Furthermore, for quality assurance, known amounts of $Ti_3C_2T_x$ MXene were digested along with the samples. Recoveries for Ti were 99%. Elemental masses were then normalized to cell number using the number of cells counted in the control wells. The surface terminations of our MXene sample not having been quantified, we estimated its molar mass by measuring the Ti proportion of a given mass of pure MXenes *via* ICP-OES, and extrapolating the corresponding molar mass. The result of 70.55% of Ti mass proportion matches well with the value of 47.867 × 3/202 = 71.09%, where 47.867 g mol^{-1} is the molar mass of Ti and 202 g mol^{-1} is the molar mass of $Ti_3C_2T_x$ MXenes as determined by Lukatskaya *et al.*[59]

Hydroxyl radical scavenging using DMSO

To study the production of hydroxyl radicals (OH^-) during irradiation with/without nanoparticles, sterile DMSO was diluted in cell medium at a concentration of 0.66 M, and added to the pre-incubated cells ~2 h before irradiation. In order to minimize the DMSO cytotoxicity, it was replaced by pure cell medium ~2 h after irradiation, just before putting the cells back into the incubator. The rest of the procedure was very similar to the radio-enhancement experiments described above. 2000 cells were seeded on 48-well plates, left to adhere for 24 h, and cell medium mixes with pre-sonicated nanoparticles were added to the wells. A control without nanoparticles was added on every plate. Each condition was measured in quadruplicates (n = 4). The outer wells of the plates were filled with 500 μl sterile PBS to achieve the same humidity in every well. The total water content was fixed at 10% in all experimental wells, in order to have the same concentration of nutrients in each condition. After 24 h of incubation, cells were washed with PBS as usual, after which DMSO in medium was added and 150 kVp X-ray irradiation took place. Cell viability was analyzed 5 days after irradiation, as usual.

The nanoparticle radiation enhancement ratio (NER) at 6 Gy irradiation is computed as follows:

$$\mathrm{NER} = \frac{\mathrm{SF}(6\ \text{Gy}, \text{no NP})}{\mathrm{SF}(6\ \text{Gy}, \text{NP})}$$

Statistical analysis

Cell viabilities and DMR data have been analysed using ANOVA and Bonferroni *post-hoc* tests to correct for multiple comparisons.

Conflicts of interest

There are no conflicts of interest to declare.

Acknowledgements

We acknowledge funding from ETH Zurich (ETH grant no. ETH-07 21-2, I. K. H.), the Swiss Cancer Research Foundation (Grant number KFS-4868-08-2019, I. K. H.), the Swiss National Science Foundation (Eccellenza grant no. 181290, I. K. H.) and the Gebauer Foundation (I. K. H.). We thank the Empa X-ray Center for providing access to their irradiation facilities, the ETH Microscopy Center ScopeM, the University of Zurich Microscopy Center for access to their microscopes and Eawag (Ralf Kägi and Andreas Voegelin) for access to the HF digestion facilities.

References

1 *Global health estimates: Leading causes of death* [Internet]. [cited on 2. Juni 2022]. Available at: **https://www.who.int/data/gho/data/themes/mortality-and-global-health-estimates/ghe-leading-causes-of-death**.
2 G. R. Dagenais, D. P. Leong, S. Rangarajan, F. Lanas, P. Lopez-Jaramillo, R. Gupta, *et al.*, Variations in common diseases, hospital admissions, and deaths in middle-aged adults in 21 countries from five continents (PURE): a prospective cohort study, *Lancet*, 2020, **395**(10226), 785–794.
3 L. A. Kunz-Schughart, A. Dubrovska, C. Peitzsch, A. Ewe, A. Aigner, S. Schellenburg, *et al.*, Nanoparticles for radiooncology: Mission, vision, challenges, *Biomaterials*, 2017, **120**, 155–184.
4 S. Bonvalot, P. L. Rutkowski, J. Thariat, S. Carrère, A. Ducassou, M. P. Sunyach, *et al.*, NBTXR3, a first-in-class radioenhancer hafnium oxide nanoparticle, plus radiotherapy versus radiotherapy alone in patients with locally advanced soft-tissue sarcoma (Act.In.Sarc): a multicentre, phase 2–3, randomised, controlled trial, *Lancet Oncol.*, 2019, **20**(8), 1148–1159.
5 S. Bonvalot, A. Gronchi, C. Le Péchoux, C. J. Swallow, D. Strauss, P. Meeus, *et al.*, Preoperative radiotherapy plus surgery versus surgery alone for patients with primary retroperitoneal sarcoma (EORTC-62092: STRASS): a multicentre, open-label, randomised, phase 3 trial, *Lancet Oncol.*, 2020, **21**(10), 1366–1377.
6 L. R. H. Gerken, A. Gogos, F. H. L. Starsich, H. David, M. E. Gerdes, H. Schiefer, *et al.*, Catalytic activity imperative for nanoparticle dose enhancement in photon and proton therapy, *Nat. Commun.*, 2022, **13**(1), 3248.
7 L. R. H. Gerken, M. E. Gerdes, M. Pruschy and I. K. Herrmann, Prospects of nanoparticle-based radioenhancement for radiotherapy, *Mater. Horiz.*, 2023, **10**, 4059–4082.
8 K. T. Butterworth, S. J. McMahon, F. J. Currell and K. M. Prise, Physical basis and biological mechanisms of gold nanoparticle radiosensitization, *Nanoscale*, 2012, **4**(16), 4830–4838.
9 Z. Kuncic and S. Lacombe, Nanoparticle radio-enhancement: principles, progress and application to cancer treatment, *Phys. Med. Biol.*, 2018, **63**(2), 02TR01.
10 D. Howard, S. Sebastian, Q. V. C. Le, B. Thierry and I. Kempson, Chemical Mechanisms of Nanoparticle Radiosensitization and Radioprotection: A Review of Structure-Function Relationships Influencing Reactive Oxygen Species, *Int. J. Mol. Sci.*, 2020, **21**(2), 579.
11 R. L. Auten and J. M. Davis, Oxygen Toxicity and Reactive Oxygen Species: The Devil Is in the Details, *Pediatr. Res.*, 2009, **66**(2), 121–127.
12 T. Helleday, E. Petermann, C. Lundin, B. Hodgson and R. A. Sharma, DNA repair pathways as targets for cancer therapy, *Nat. Rev. Cancer*, 2008, **8**(3), 193–204.
13 M. E. Lomax, L. K. Folkes and P. O'Neill, Biological Consequences of Radiation-induced DNA Damage: Relevance to Radiotherapy, *Clin. Oncol.*, 2013, **25**(10), 578–585.
14 R. Baskar, J. Dai, N. Wenlong, R. Yeo and K. W. Yeoh, Biological response of cancer cells to radiation treatment, *Front. Mol. Biosci.*, 2014, **1**, 24.
15 S. Penninckx, A. C. Heuskin, C. Michiels and S. Lucas, Gold Nanoparticles as a Potent Radiosensitizer: A Transdisciplinary Approach from Physics to Patient, *Cancers*, 2020, **12**(8), 2021.
16 J. Schuemann, A. F. Bagley, R. Berbeco, K. Bromma, K. T. Butterworth, H. L. Byrne, *et al.*, Roadmap for metal nanoparticles in radiation therapy: current status, translational challenges, and future directions, *Phys. Med. Biol.*, 2020, **65**(21), 21RM02.
17 J. F. Hainfeld, D. N. Slatkin and H. M. Smilowitz, The use of gold nanoparticles to enhance radiotherapy in mice, *Phys. Med. Biol.*, 2004, **49**(18), N309–N315.
18 E. Brun, L. Sanche and C. Sicard-Roselli, Parameters governing gold nanoparticle X-ray radiosensitization of DNA in solution, *Colloids Surf., B*, 2009, **72**(1), 128–134.
19 J. F. Hainfeld, F. A. Dilmanian, Z. Zhong, D. N. Slatkin, J. A. Kalef-Ezra and H. M. Smilowitz, Gold nanoparticles enhance the radiation therapy of a murine squamous cell carcinoma, *Phys. Med. Biol.*, 2010, **55**(11), 3045–3059.
20 Y. Zheng, D. J. Hunting, P. Ayotte and L. Sanche, Radiosensitization of DNA by Gold Nanoparticles Irradiated with High-Energy Electrons, *Radiat. Res.*, 2008, **169**(1), 19–27.
21 K. W. Fornalski, Simple empirical correction functions to cross sections of the photoelectric effect, Compton scattering, pair and triplet production for carbon radiation shields for intermediate and high photon energies, *J. Phys. Commun.*, 2018, **2**(3), 035038.
22 A. Fujishima, T. N. Rao and D. A. Tryk, Titanium dioxide photocatalysis, *J. Photochem. Photobiol., C*, 2000, **1**(1), 1–21.
23 A. M. Jastrzębska, A. Szuplewska, T. Wojciechowski, M. Chudy, W. Ziemkowska, L. Chlubny, *et al.*, In vitro studies on cytotoxicity of delaminated Ti_3C_2 MXene, *J. Hazard. Mater.*, 2017, **339**, 1–8.
24 X. Han, J. Huang, H. Lin, Z. Wang, P. Li and Y. Chen, 2D Ultrathin MXene-Based Drug-Delivery Nanoplatform for

Synergistic Photothermal Ablation and Chemotherapy of Cancer, *Adv. Healthcare Mater.*, 2018, **7**(9), 1701394.

25 M. Naguib, M. Kurtoglu, V. Presser, J. Lu, J. Niu, M. Heon, *et al.*, Two-Dimensional Nanocrystals Produced by Exfoliation of Ti_3AlC_2, *Adv. Mater.*, 2011, **23**(37), 4248–4253.

26 J. Xuan, Z. Wang, Y. Chen, D. Liang, L. Cheng, X. Yang, *et al.*, Organic-Base-Driven Intercalation and Delamination for the Production of Functionalized Titanium Carbide Nanosheets with Superior Photothermal Therapeutic Performance, *Angew. Chem., Int. Ed.*, 2016, **55**(47), 14569–14574.

27 G. Liu, J. Zou, Q. Tang, X. Yang, Y. Zhang, Q. Zhang, *et al.*, Surface Modified Ti_3C_2 MXene Nanosheets for Tumor Targeting Photothermal/Photodynamic/Chemo Synergistic Therapy, *ACS Appl. Mater. Interfaces*, 2017, **9**(46), 40077–40086.

28 H. Lin, Y. Wang, S. Gao, Y. Chen and J. Shi, Theranostic 2D Tantalum Carbide (MXene), *Adv. Mater.*, 2018, **30**(4), 1703284.

29 K. Rasool, M. Helal, A. Ali, C. E. Ren, Y. Gogotsi and K. A. Mahmoud, Antibacterial Activity of $Ti_3C_2T_x$ MXene, *ACS Nano*, 2016, **10**(3), 3674–3684.

30 C. E. Shuck, A. Sarycheva, M. Anayee, A. Levitt, Y. Zhu, S. Uzun, *et al.*, Scalable Synthesis of Ti3C2Tx MXene, *Adv. Eng. Mater.*, 2020, **22**(3), 1901241.

31 G. Valurouthu, K. Maleski, N. Kurra, M. Han, K. Hantanasirisakul, A. Sarycheva, *et al.*, Tunable electrochromic behavior of titanium-based MXenes, *Nanoscale*, 2020, **12**(26), 14204–14212.

32 A. C. Carreira, R. F. de Almeida and L. C. Silva, Development of lysosome-mimicking vesicles to study the effect of abnormal accumulation of sphingosine on membrane properties, *Sci. Rep.*, 2017, **7**(1), 3949.

33 F. Xia, J. Lao, R. Yu, X. Sang, J. Luo, Y. Li, *et al.*, Ambient oxidation of Ti3C2 MXene initialized by atomic defects, *Nanoscale*, 2019, **11**(48), 23330–23337.

34 A. Iqbal, J. Hong, T. Y. Ko and C. M. Koo, Improving oxidation stability of 2D MXenes: synthesis, storage media, and conditions, *Nano Convergence*, 2021, **8**(1), 9.

35 T. Habib, X. Zhao, S. A. Shah, Y. Chen, W. Sun, H. An, *et al.*, Oxidation stability of Ti3C2Tx MXene nanosheets in solvents and composite films, *npj 2D Mater. Appl.*, 2019, **3**(1), 1–6.

36 C. J. Zhang, S. Pinilla, N. McEvoy, C. P. Cullen, B. Anasori, E. Long, *et al.*, Oxidation Stability of Colloidal Two-Dimensional Titanium Carbides (MXenes), *Chem. Mater.*, 2017, **29**(11), 4848–4856.

37 O. Mashtalir, K. M. Cook, V. N. Mochalin, M. Crowe, M. W. Barsoum and Y. Gogotsi, Dye adsorption and decomposition on two-dimensional titanium carbide in aqueous media, *J. Mater. Chem. A*, 2014, **2**(35), 14334–14338.

38 S. Huang and V. N. Mochalin, Combination of High pH and an Antioxidant Improves Chemical Stability of Two-Dimensional Transition-Metal Carbides and Carbonitrides (MXenes) in Aqueous Colloidal Solutions, *Inorg. Chem.*, 2022, **61**(26), 9877–9887.

39 K. Doudrick, O. Monzón, A. Mangonon, K. Hristovski and P. Westerhoff, Nitrate Reduction in Water Using Commercial Titanium Dioxide Photocatalysts (P25, P90, and Hombikat UV100), *J. Environ. Eng.*, 2012, **138**(8), 852–861.

40 L. R. H. Gerken, A. L. Neuer, P. M. Gschwend, K. Keevend, A. Gogos, A. H. C. Anthis, *et al.*, Scalable Synthesis of Ultrasmall Metal Oxide Radio-Enhancers Outperforming Gold, *Chem. Mater.*, 2021, **33**(9), 3098–3112.

41 H. Geng, Y. Ren, G. Qin, T. Wen, Q. Liu, H. Xu, *et al.*, Ti3C2 nanosheets with broad-spectrum antioxidant activity for cytoprotection against oxidative stress, *RSC Adv.*, 2022, **12**(18), 11128–11138.

42 A. Szuplewska, A. Rozmysłowska-Wojciechowska, S. Poźniak, T. Wojciechowski, M. Birowska, M. Popielski, *et al.*, Multilayered stable 2D nano-sheets of Ti2NTx MXene: synthesis, characterization, and anticancer activity, *J. Nanobiotechnol.*, 2019, **17**(1), 114.

43 A. L. Neuer, L. R. H. Gerken, K. Keevend, A. Gogos and I. K. Herrmann, Uptake, distribution and radio-enhancement effects of gold nanoparticles in tumor microtissues, *Nanoscale Adv.*, 2020, **2**(7), 2992–3001.

44 A. L. Neuer, A. Jessernig, L. R. H. Gerken, A. Gogos, F. H. L. Starsich, A. H. C. Anthis, *et al.*, Cellular fate and performance of group IV metal organic framework radioenhancers, *Biomater. Sci.*, 2022, **10**, 6558–6569.

45 A. Jastrzębska, A. Szuplewska, A. Rozmysłowska-Wojciechowska, M. Chudy, A. Olszyna, M. Birowska, *et al.*, On tuning the cytotoxicity of Ti3C2 (MXene) flakes to cancerous and benign cells by post-delamination surface modifications, *2D Mater.*, 2020, **7**(2), 025018.

46 Y. Li, H. Yuan, A. von dem Bussche, M. Creighton, R. H. Hurt, A. B. Kane, *et al.*, Graphene microsheets enter cells through spontaneous membrane penetration at edge asperities and corner sites, *Proc. Natl. Acad. Sci. U. S. A.*, 2013, **110**(30), 12295–12300.

47 M. Kucki, L. Diener, N. Bohmer, C. Hirsch, H. F. Krug, V. Palermo, *et al.*, Uptake of label-free graphene oxide by Caco-2 cells is dependent on the cell differentiation status, *J. Nanobiotechnol.*, 2017, **15**(1), 46.

48 Z. Tu, K. Achazi, A. Schulz, R. Mülhaupt, S. Thierbach, E. Rühl, *et al.*, Combination of Surface Charge and Size Controls the Cellular Uptake of Functionalized Graphene Sheets, *Adv. Funct. Mater.*, 2017, **27**(33), 1701837.

49 P. Foroozandeh and A. A. Aziz, Insight into Cellular Uptake and Intracellular Trafficking of Nanoparticles, *Nanoscale Res. Lett.*, 2018, **13**(1), 339.

50 D. Manzanares and V. Ceña, Endocytosis: The Nanoparticle and Submicron Nanocompounds Gateway into the Cell, *Pharmaceutics*, 2020, **12**(4), 371.

51 J. Mosquera, I. García and L. M. Liz-Marzán, Cellular Uptake of Nanoparticles versus Small Molecules: A Matter of Size, *Acc. Chem. Res.*, 2018, **51**(9), 2305–2313.

52 S. Barua and S. Mitragotri, Challenges associated with penetration of nanoparticles across cell and tissue barriers:

A review of current status and future prospects, *Nano Today*, 2014, **9**(2), 223–243.

53 S. J. McMahon, The linear quadratic model: usage, interpretation and challenges, *Phys. Med. Biol.*, 2018, **64**(1), 01TR01.

54 C. Korupalli, K. L. You, G. Getachew, A. S. Rasal, W. B. Direrssa, M. Zakki Fahmi, *et al.*, Engineering the Surface of Ti3C2 MXene Nanosheets for High Stability and Multimodal Anticancer Therapy, *Pharmaceutics*, 2022, **14**(2), 304.

55 B. Perillo, M. Di Donato, A. Pezone, E. Di Zazzo, P. Giovannelli, G. Galasso, *et al.*, ROS in cancer therapy: the bright side of the moon, *Exp. Mol. Med.*, 2020, **52**(2), 192–203.

56 K. Rajavel, S. Shen, T. Ke and D. Lin, Achieving high bactericidal and antibiofouling activities of 2D titanium carbide (Ti3C2Tx) by delamination and intercalation, *2D Mater.*, 2019, **6**(3), 035040.

57 S. Bonvalot, P. L. Rutkowski, J. Thariat, S. Carrere, M. P. Sunyach, E. Saada, *et al.*, A phase II/III trial of hafnium oxide nanoparticles activated by radiotherapy in the treatment of locally advance soft tissue sarcoma of the extremity and trunk wall, *Ann. Oncol.*, 2018, **29**, viii753.

58 A. Subiel, R. Ashmore and G. Schettino, Standards and Methodologies for Characterizing Radiobiological Impact of High-Z Nanoparticles, *Theranostics*, 2016, **6**(10), 1651–1671.

59 M. R. Lukatskaya, S. M. Bak, X. Yu, X. Q. Yang, M. W. Barsoum and Y. Gogotsi, Probing the Mechanism of High Capacitance in 2D Titanium Carbide Using In Situ X-Ray Absorption Spectroscopy, *Adv. Energy Mater.*, 2015, **5**(15), 1500589.